

# Study of the Mechanical Properties of Myomesin Proteins Using Dynamic Force Spectroscopy

P. Bertoncini<sup>1\*</sup>, R. Schoenauer<sup>2</sup>, I. Agarkova<sup>2</sup>, M. Hegner<sup>1</sup>, J.-C. Perriard<sup>2</sup> and H.-J. Güntherodt<sup>1</sup>

<sup>1</sup>*Institute of Physics, University of Basel, Klingelbergstrasse 82 CH-4056 Basel, Switzerland*

<sup>2</sup>*Institute of Cell Biology, ETH-Zürich Hönggerberg CH-8093 Zürich, Switzerland*

Myomesin is the most prominent structural component of the sarcomeric M-Band that is expressed in mammalian heart and skeletal muscles. Like titin, this protein is an intracellular member of the Ig-fibronectin superfamily, which has a flexible filamentous structure and which is largely composed of two types of domain that are similar to immunoglobulin (Ig)-like and fibronectin type III (FNIII) domains. Several myomesin isoforms have been identified, and their expression patterns are highly regulated both spatially and temporally. Particularly, alternative splicing in the central part of the molecule gives rise to an isoform, EH (embryonic heart)-myomesin, containing a serine and proline-rich insertion with no well-defined secondary structure, the EH segment. EH-myomesin represents the major myomesin isoform at embryonic stages of mammalian heart and is rapidly down-regulated around birth, but it is re-expressed in the heart of patients suffering from dilated cardio-myopathy. Here, in order to facilitate a better understanding of the physiological, and possibly pathological, functions of myomesin proteins, we explore the mechanical stability, elasticity and force-driven structural changes of human myomesin's sub-molecular segments using single-molecule force spectroscopy and protein engineering. We find that human myomesin molecules are composed of modules (Ig and FNIII), that are designed to withstand force and we demonstrate that the human cardiac EH segment functions like an additional elastic stretch in the middle part of the EH-myomesin and behaves like a random coil. Consequently myomesin isoforms (proteins with or without the EH segment) have different elastic properties, the EH-myomesin being the more compliant one. These findings imply that the compliance of the M-band increases with the amount of EH-myomesin it contains. So, we provide the evidence that not only titin but also other sarcomeric proteins have complicated visco-elastic properties depending on the contractile parameters in different muscle types.

© 2005 Elsevier Ltd. All rights reserved.

**Keywords:** myomesin; EH-myomesin; EH segment; M-band; mechanical unfolding

\*Corresponding author

## Introduction

Striated muscle is an efficient and precise machine that contains complex interconnected cytoskeletal networks. Its characteristic striated appearance results directly from the precise align-

ment of the filament systems of the sarcomere, the basic contractile unit of myofibrils. The principle components of the contractile apparatus include parallel arrays of actin-containing thin filaments and myosin-containing thick filaments. During muscle contraction, both filaments slide past one another, shortening the entire length of the sarcomere. This efficient macroscopic motion is generated by molecular interactions produced by actin and myosin in each sarcomere.<sup>1</sup>

During contraction or extension sarcomeric shape and dimensions may change in sarcomeric length as well as in cross-sectional area, while maintaining

Abbreviations used: Ig, immunoglobulin; FNIII, fibronectin type III; EH, embryonic heart; MDa, megadalton; AFM, atomic force microscopy; pN, picoNewton; WLC, worm-like-chain.

E-mail address of the corresponding author: [Bertoncini.Patricia@wanadoo.fr](mailto:Bertoncini.Patricia@wanadoo.fr)

the structural integrity of the sarcomere. When a relaxed sarcomere is stretched, a passive elastic force is generated that restores sarcomeric dimensions following release.<sup>2</sup> Two main systems are involved in the control mechanisms that provide spatial order of the force-producing proteins, myosin and actin. The first is the giant filamentous protein titin that probably controls the resting length<sup>†</sup> of the sarcomere and the operating range<sup>‡</sup> of sarcomere lengths and that might function to stabilize the position of the thick filaments at the center of the sarcomere during activation.<sup>3–6</sup> The second is the sarcomeric M-band, a transverse region at the midpoint of the sarcomere that might ensure the maintenance of the hexagonal cross-sectional lattice and the lateral alignment of individual thick filaments of the contractile apparatus of cross-striated myofibrils. Within the M-line, myomesin and M-protein are the main proteins that cross-link thick filaments transversely.<sup>7</sup> Myomesin is the most prominent structural component of the sarcomeric M-band, since it is expressed in all types of striated muscle, while M-protein is restricted to the M-lines of fast muscle fiber types and cardiac muscle. So myomesin is believed to be involved in general mechanisms controlling the assembly and maintenance of the M-band structure.<sup>1,8</sup>

The titin molecule is a flexible filament that spans half the sarcomere and is composed of a single polypeptide. The molecular mass of soleus skeletal titin is 3.7 MDa,<sup>5,9</sup> the total coding capacity of the human titin gene is 4.2 MDa (accession AJ277892<sup>10</sup>). In different muscle types different length isoforms of titin are expressed.<sup>6,11</sup> The A-band part of titin contains the largest part of the molecule and the sequence is highly conserved, both between different muscle types and in different species. It comprises super-repeats of immunoglobulin (Ig) and fibronectin type III (FNIII) globular domains and is thought to play an important role as a scaffold.<sup>11</sup> The I-band region corresponds to the elastic part of the titin molecule. The intrinsic property of muscle, that consists of maintaining the overlap of the thin and thick filaments when inactivated myofibrils are stretched beyond or shortened below their resting (slack) length, is specifically attributed to this region of titin. Both the contour length of this region and its intrinsic extensible properties are the main determinants of the so-called passive tension. The amino-terminal (or “proximal”) and carboxy-terminal (or “distal”) I-band segments contain Ig domains that are arranged in tandem and conserved between isoforms. The part joining them is isoform-dependent and varies greatly in structure and size. It has three sub-regions: an additional segment of tandem Ig domains, the unique PEVK region, which is named

on the basis of its abundance of proline (P), glutamate (E), valine (V) and lysine (K) residues<sup>11</sup> and the N2 region. There are two alternative forms of N2 region, N2A and N2B. Skeletal titins contain N2A sequences, whereas cardiac titins contain N2B or both N2A and N2B sequences. N2 region differs only between skeletal and cardiac muscles and the size of the Ig segments and PEVK region varies between all muscle types.<sup>11,6</sup> Relatively extensible muscles, such as the skeletal soleus, contain larger titin isoforms that have longer and more compliant I-band. Stiffer muscles, such as cardiac muscles, have smaller isoforms with shorter and stiffer I-band parts.<sup>4,5,12</sup> In particular, it was found that the length of the PEVK sequence in titin isoforms correlates with muscle stiffness.<sup>13</sup> The complex structure-dependent elasticity of titin was established by both *in situ*<sup>13–17</sup> and single molecule experiments<sup>18–28</sup> and these studies indicate that the elastic properties of the titin molecule can be explained by the “sum of its parts”. That means that, upon physiological stretching of the sarcomere, the distinct titin I-band spring elements appear to be recruited in a sequential order: the tandem-Ig segment elongates at lower forces, whereas at higher forces and greater stretch, the PEVK region unravels and, in cardiac muscle, the N2B unique sequence (third spring element) extends upon still higher levels of stretch.

The myomesin molecule has a mass of ~185 kDa and has a flexible filamentous structure. It is largely composed of two types of domain that are similar to (Ig)-like and (FNIII) domains.<sup>29</sup> Several myomesin isoforms have been identified, and their expression patterns are highly regulated both spatially and temporally. Particularly, alternative splicing in the central part of the molecule gives rise to an isoform, EH (embryonic heart)-myomesin, containing a serine and proline-rich insertion with no well-defined secondary structure, the EH segment. EH-myomesin represents the major myomesin isoform at embryonic stages of mammalian heart and is rapidly down-regulated around birth (its sequence is identical to the previously identified skelemin sequence<sup>30</sup>). It is re-expressed in the heart of patients suffering from dilated cardiomyopathy.<sup>31</sup> The total amount of myomesin in the sarcomere (irrespective of the presence or absence of the EH fragment) remains roughly the same in all kinds of striated muscle, but the proportion between both isoforms is muscle fiber type-dependent. Two extreme cases are observed, where one isoform is present: only EH-myomesin is expressed in the M-bands of the embryonic heart sarcomere, whereas in M-bands of fast muscle sarcomere, all myomesin molecules do not have any EH fragment. So the molecular composition of the sarcomeric M-band correlates with muscle fiber type.<sup>31</sup>

In order to facilitate a better understanding of the physiological, and possibly pathological, functions of myomesin proteins, we explore the mechanical stability, elasticity and force-driven structural changes of human myomesin's sub-molecular

<sup>†</sup> Resting length: length to which the relaxed sarcomeres freely shorten in the absence of external load.

<sup>‡</sup> Operating range: length over which sarcomeres shorten and extend in muscle *in vivo*.

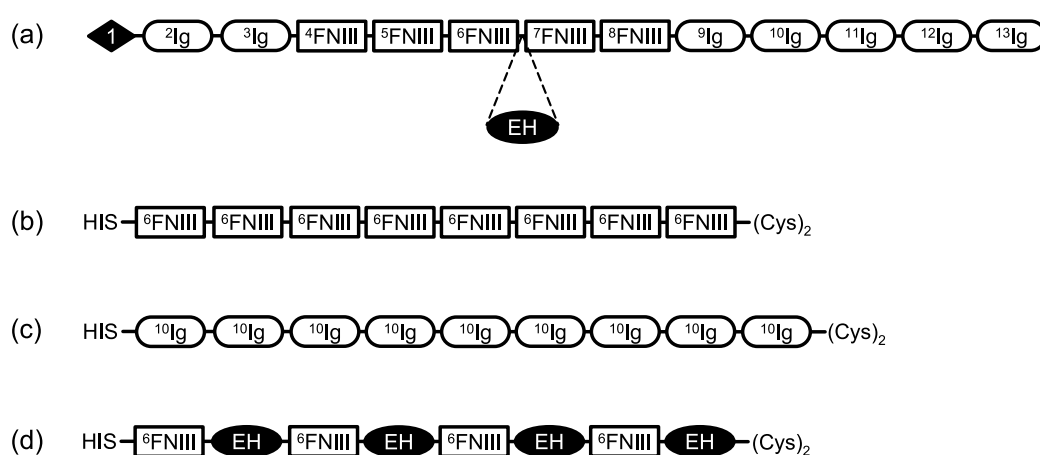


**Figure 1.** Schematic diagrams of the modular structure of myomesin isoforms (a) and illustrations of multi-modular protein constructs ((b)–(d)).

segments using single-molecule force spectroscopy and protein engineering.

## Results and Discussion

Here, we use an atomic force microscope (AFM) in the force-measuring mode to measure the mechanical properties of myomesin's domains. In a typical experiment, a single protein is stretched for up to several hundred nanometers between a microscopic silicon nitride tip of a flexible cantilever and a flat substrate that is mounted on a highly accurate piezoelectric positioner.<sup>20,27,32,33</sup> With the development of protein engineering techniques, not only native proteins can be studied but also well-designed and constructed poly-proteins.<sup>21,34–36</sup> This allows a precise analysis of the mechanical unfolding of specific domains and identification of their mechanical “fingerprints” due to the fact that they have a perfect repetitive structure that results in a unique periodical sawtooth pattern in force-extension recordings.

Here, we explore in detail the mechanical behavior of three individual human myomesin domains: a fibronectin type III domain <sup>6</sup>FNIII, an immunoglobulin-like domain <sup>10</sup>Ig, and a serine/proline-rich domain, the EH-segment. A schematic representation of the mammalian myomesin proteins can be seen in Figure 1(a). One myomesin protein is composed of seven Ig domains and five FNIII domains. <sup>6</sup>FNIII and <sup>10</sup>Ig correspond to the sixth and the tenth domain of the myomesin molecule, respectively, and the EH segment is the additional fragment inserted between domains 6 and 7 of the EH-myomesin isoform.

### Mechanical stability of fibronectin type III (<sup>6</sup>FNIII) and immunoglobulin-like domain (<sup>10</sup>Ig)

First, two homomeric poly-proteins, (<sup>6</sup>FNIII)<sub>8</sub> and (<sup>10</sup>Ig)<sub>9</sub>, containing tandem repeats of a single <sup>6</sup>FNIII domain and of a single <sup>10</sup>Ig domain, were constructed using protein engineering techniques to

construct different poly-proteins<sup>21</sup> (see Materials and Methods) and their mechanical behavior investigated (see Figure 1(b) and (c)). Stretching these proteins with AFM results in characteristic fingerprints: each force-extension trace shows a characteristic sawtooth pattern, in which stretching of the unfolded length of a protein causes a slow rise in force, followed by a sudden drop as each domain unfolds (examples of traces, recorded at a pulling speed of 500 nm/s are given in Figure 2(a) for (<sup>6</sup>FNIII)<sub>8</sub> and in Figure 2(b) for (<sup>10</sup>Ig)<sub>9</sub>). An initial peak can be observed as the tip lifts off the surface (zero extension in Figure 2(b)), and is attributed to the interaction of the tip with the surface or proteins on the surface. As the N-terminal end of the protein is non-specifically attached to the tip, it may become attached at different points along the length of the poly-protein, resulting in different numbers of equally spaced force peaks in different pulls. In Figure 2(a) and (b), as many as eight peaks can be seen for (<sup>6</sup>FNIII)<sub>8</sub> (Figure 2(a)) and six peaks for (<sup>10</sup>Ig)<sub>9</sub> (Figure 2(b)). Although the protein (<sup>10</sup>Ig)<sub>9</sub> contains nine domains, the maximum number we have observed is six (Figure 2(b)). Detachment of the protein from the tip is responsible for the final peak.

The force at which an unfolding event occurs reflects the mechanical stability of a particular folded domain under the specific experimental conditions used. The unfolding force, and therefore the mechanical stability, depends on the pulling rate of extension; the faster the pulling speed, the higher the force required to cause the unfolding of the domain. An example of a histogram of the unfolding forces for one set of data collected at a pulling speed of 500 nm/s for the <sup>6</sup>FNIII octamer is given in Figure 2(c). The force distribution shows a peak at ~161 pN ( $n=132$ ). The dependence of <sup>6</sup>FNIII and <sup>10</sup>Ig unfolding forces on pulling speed can be seen in Figure 2(d). The graph shows the average unfolding forces measured while pulling the poly-proteins at different pulling speeds and in different sets of experiments ( $\blacksquare$ ,  $\circ$ ,  $\blacktriangle$  for (<sup>6</sup>FNIII)<sub>8</sub> and  $\blacksquare$ ,

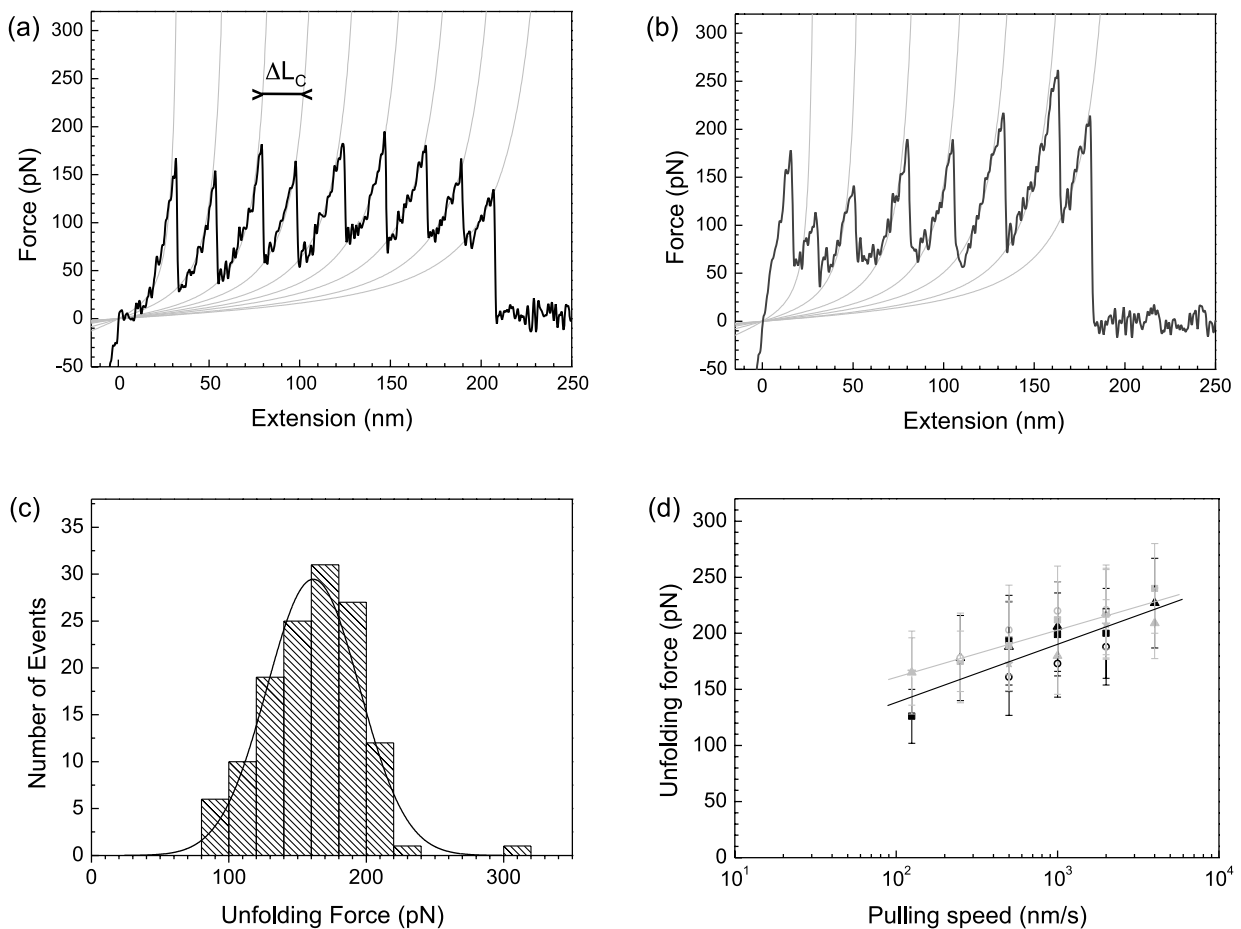


**Figure 2.** Mechanical stability of domain  ${}^6\text{FNIII}$  and  ${}^{10}\text{Ig}$ . (a) and (b) Stretching of  ${}^6\text{FNIII}_8$  and  ${}^{10}\text{Ig}_9$  poly-proteins produces a force-extension curve showing the characteristic sawtooth pattern of unfolding. The force-extension curves show different number of sawteeth, depending on the number of modules picked up by the AFM tip. The continuous lines are fits of the WLC model of polymer elasticity to the data. The pulling speed is 500 nm/s. (c) Frequency histogram of unfolding forces of the  ${}^6\text{FNIII}$  domain at a pulling speed of 500 nm/s (peak centered at  $\sim 160$  pN ( $161$  pN ( $\pm 34$  pN),  $n=132$ )). (d) The force required to unfold a domain is dependent on the pulling speed. The Figure shows the average unfolding forces measured while pulling segments of  ${}^6\text{FNIII}_9$  and  ${}^{10}\text{Ig}_9$  poly-proteins at different speeds. The graph shows the result of three and four different experiments for  ${}^6\text{FNIII}_8$  (black symbols) and for  ${}^{10}\text{Ig}_9$  (gray symbols), respectively. Error bars are in the range of  $\pm 40$  pN.

$\circ, \blacktriangle, \star$  for  ${}^{10}\text{Ig}_9$ . For pulling speeds ranging from 125 nm/s to 4000 nm/s, forces that unfold  ${}^6\text{FNIII}$  and  ${}^{10}\text{Ig}$  domains were in the region 126–227 pN and 150–240 pN, respectively. The unfolding forces increased linearly with the logarithm of stretch rate, but the stretch-rate dependence of unfolding forces was stronger in  ${}^6\text{FNIII}_8$  than in  ${}^{10}\text{Ig}_9$ . These results are in agreement with other studies published previously, where the mechanical properties of fibronectin type III<sup>37–40</sup> and of immunoglobulin domains<sup>20,24,26,37,41</sup> were studied. It was shown that forces that unfold FNIII domains originating from the A-band titin and from fibronectin protein are in the region 100–200 pN at force-loading rates of 50 to 1000 nm/s<sup>37</sup> and in the region 75–200 pN at a pulling speed of 600 nm/s,<sup>40</sup> respectively. Typically, Ig domains unfold at 150–300 pN at force-loading rates of 50 to 1000 nm/s.<sup>37</sup> Different mechanical properties of Ig domains were found within the I-band part of titin: the proximal tandem region contains most of the weak Ig domains, with averaged unfolding forces of

150–200 pN,<sup>24,26</sup> the differentially expressed domains, which are centrally positioned in the I-band, have intermediate stability and unfolding forces of  $\sim 200$  pN<sup>26,37</sup> and the distal segment contains the strongest domains, with unfolding force of  $\sim 150$ –300 pN.<sup>20,24,26,37</sup>

Consecutive force-peaks were fitted by the Worm-Like Chain (WLC) model of polymer elasticity<sup>42,43</sup> to determine the contour-length gain accompanying domain unfolding events (see Materials and Methods). For each molecule, the value of the persistence length  $p$  was chosen to give the best agreement with the data in the complete force range of up to 200 pN and this value was used to fit the consecutive force-peaks (it was not possible to allow  $p$  to vary freely for the fit to each force peak, as the values of the other fitted parameters then became less meaningful). The average contour length increment and its standard deviation in the  ${}^6\text{FNIII}$  octamer are  $\Delta L_C = 26.3$  ( $\pm 1.3$ ) nm (calculated with 724 length increments

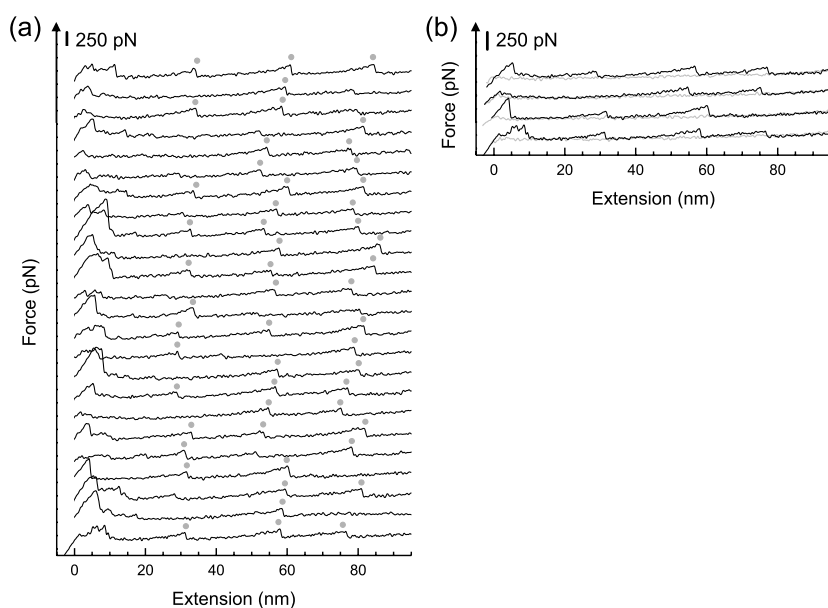


**Figure 3.** Repeated unfolding-refolding of  $({}^6\text{FNIII})_8$  poly-protein recorded at a pulling speed of 500 nm/s. The curves were obtained by stretching and relaxing the same molecule multiple times. (a) The unfolding traces of the unfolding-refolding cycles. The gray dots mark the position where unfolding occurs. (b) Three complete unfolding and refolding cycles are shown. The curves corresponding to the unfolding are presented in black, the one corresponding to the refolding in gray. The force curves in these plots are shifted vertically for clarity, so they do not share a common zero force level.

between force peaks from 163 different molecules, see Figure 2(a), gray lines for example) and in the  ${}^{10}\text{Ig}$  multimer are  $\Delta L_C = 27.9 (\pm 1.5)$  nm (calculated with 364 length increments between force peaks from 120 different molecules, see Figure 2(b), gray lines for example). This is consistent with the number of residues per domain in  ${}^{10}\text{Ig}$  and in  ${}^6\text{FNIII}$  ( $\sim 90$  residues) since the interval between peaks is correlated to the length of the “folded core” of the domain.<sup>34,35</sup> In the case of the I91 titin’s I-band domain (titin I27 $\dagger$ , corresponding to I91 $\ddagger$  in AJ277892), the folded core encompasses about 72 amino acid residues and the observed distance between peaks corresponds to 70 amino acid residues although the I91 domain has a total of 89 amino acid residues.<sup>34,35</sup>

Persistence lengths were in the range of 0.36 ( $\pm 0.10$ ) nm to give the best agreement with the data. Nevertheless, there are deviations, especially in the low-force regime. This reflects the problems in describing by a single parameter  $p$  the complicated elasticity of a real polymer over the complete force range (0–300 pN).<sup>20,21,37,42,44</sup>

A characteristic feature of these traces is the increase in the force required to unfold each successive domain in the chain, as chain extension progresses. In the case of  ${}^6\text{FNIII}$  domain, the unfolding forces range from about 150 to 190 pN as can be seen in Figure 2(a). By considering the height of each individual force-peak corresponding to the unfolding of one domain as a function of its position in the sawtooth pattern, we observe a tendency for early force-peaks to have smaller unfolding forces where the last peak is about 25% ( $\sim 40$  pN) higher in force than the first. We measure an average slope of  $\sim 7.4 (\pm 0.6)$  pN/peak. This value is consistent with previously published ones

on homomeric poly-proteins.<sup>21,40</sup> Previous theoretical studies on the unfolding behavior of identical domains linked in series predict that the resulting sawtooth pattern should show a hierarchical relationship due to the decrease in unfolding probability, as more domains unfold.<sup>45–47</sup> In the case of  ${}^{10}\text{Ig}$  domains, an average increase of  $15 (\pm 0.9)$  pN/peak is measured, which the theoretical considerations above are not sufficient to explain. This value is surprisingly closer to those obtained for heterogeneous proteins: 16.2 pN/peak when stretching the native FNIII region of fibronectin,<sup>40</sup> around 15 pN/peak (12 pN/peak) and 21 pN/peak (31 pN/peak) when unfolding Ig segments originating from the proximal and the distal tandem region of the I-band titin, respectively.<sup>24,26</sup>

The poly-proteins  $({}^6\text{FNIII})_8$  and  $({}^{10}\text{Ig})_9$  were stretched and relaxed repeatedly while limiting the total extension of the molecule to prevent its detachment from the AFM tip in order to investigate the reversibility of the unfolding-refolding. In a typical experiment, a protein segment is first stretched, allowing its characteristic sawtooth pattern to become apparent and consequently counting of the available folded domains. After reaching the extended state, the protein segment is relaxed to its initial contour length. After a variable time period ( $\Delta t$ ), the protein is stretched again, and several unfolding peaks are observed. Some of the domains that unfolded at the first extension have refolded on relaxation. Both  ${}^6\text{FNIII}$  and  ${}^{10}\text{Ig}$  domains are able to refold after being unfolded mechanically. For illustration, 24 unfolding traces of the unfolding-refolding cycles and three complete unfolding and refolding cycles obtained when stretching a  $({}^6\text{FNIII})_8$  protein (with  $\Delta t = 1.5$  s) can be seen in Figure 3(a) and (b), respectively. The force curves in these plots are shifted vertically for clarity, so they do not share a common zero force level. The number of discernable unfolding events varies

$\dagger$  Nomenclature of Labeit S. & Kolmerer B. (1995).<sup>11</sup>

$\ddagger$  Nomenclature of Bang M.- L. *et al.* (2001).<sup>10</sup>

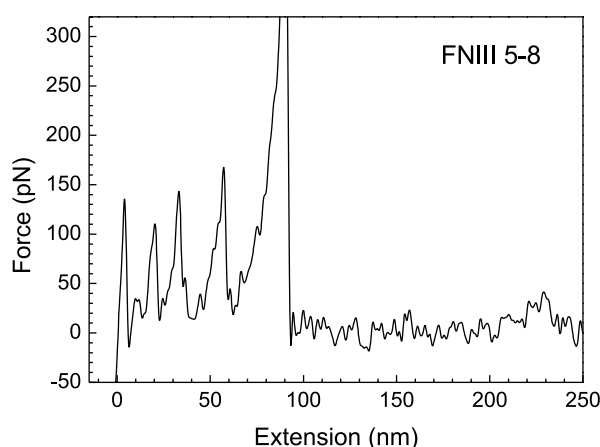


**Figure 4.** Mechanical stability of  $^5\text{FNIII}$ - $^8\text{FNIII}$  domains captured by single-molecule spectroscopy. Example of a force-extension curve of a recombinant myomesin protein containing FNIII domains 5–8 at a pulling speed of 500 nm/s.

from one stretch to the other. We observe that the number of discernable unfolding events increases with  $\Delta t$ , indicative of the fact that the protein needs time to refold in its native conformation, as observed for titin domains<sup>20,21</sup> and FNIII tenascin.<sup>38</sup> An elegant way to monitor and study the folding trajectories of a single protein was recently published by Fernandez *et al.*<sup>48</sup> The authors used force-clamp atomic force microscopy (see also Oberhauser *et al.*<sup>49</sup>) to measure the end-to-end length of a protein during its folding reaction at the single molecule level and show that the time to fold was dependent on the contour length of the unfolded protein and the stretching force applied during folding.

In order to complete these results, we decided to pull a protein made of other fibronectin type III domains originating from myomesin. An example of a force-extension curve of a recombinant protein containing FNIII domains 5–8 is presented in Figure 4. A sawtooth pattern corresponding to the sequential unfolding of individual FNIII domains can be seen. So, several myomesin domains (FNIII and Ig) are mechanically stable.

#### Identification and measurement of the elasticity of an EH segment

Second, a chimeric poly-protein, composed of four identical repeats of  $^6\text{FNIII-EH}$ , a unit containing the sixth module of human myomesin linked to the human EH segment was synthesized (see Materials and Methods). A schematic representation of this molecule is shown in Figure 1(d). This engineered protein,  $(^6\text{FNIII-EH})_4$ , combines the uncertain structure of the EH segment with the  $^6\text{FNIII}$  domain characterized above, that therefore provides a useful internal reference. This experimental design is based on the discovery that the unfolding of tandem protein modules follows their

mechanical stability rather than their relative positioning in the polypeptide chain (the less stable unfold first)<sup>50</sup> and on the fact that single-molecule techniques can help in elucidating the conformation of proteins that lack a well-defined structure, as in the case of the PEVK and N2B fragments of human cardiac titin<sup>22–25</sup> and in the case of barnase.<sup>51</sup>

In this part of the study, we have to compare in detail the fingerprints obtained on the homomeric poly-protein  $(^6\text{FNIII})_8$  and those obtained on the chimeric protein  $(^6\text{FNIII-EH})_4$ . For this purpose, let us start with a close examination of the force-extension curves recorded on  $(^6\text{FNIII})_8$ . By fitting the WLC-model of elasticity<sup>43</sup> to the initial part of the force-extension curves, before any unfolding event is observed, we can determine the folded length of the proteins  $L_0$ . We find that the folded length of a poly-protein depends on the number of modules picked up by the AFM tip ( $n$ ) and the folded length of a single module, as in the study of the conformation of the PEVK segment of titin published by Li *et al.*<sup>22</sup> As an example, two force-extension curves, recorded at a pulling speed of 500 nm/s, where four and eight unfolding peaks can be seen in Figure 5(a). A plot of  $L_0$  versus  $n$  (Figure 5(b)) exhibits a slope of  $3.7(\pm 0.7)$  nm/module.

Figure 5(c) shows several force-extension curves for the  $(^6\text{FNIII-EH})_4$  poly-protein at a pulling speed of 500 nm/s.  $^6\text{FNIII}$  domains are easily identified due to their characteristic unfolding force and their contour length increment between two consecutive peaks. Different numbers of  $^6\text{FNIII}$  unfolding peaks (one, two, three or four) can be seen, excluding the last peak that corresponds to the detachment of the molecule from the AFM tip. Because the EH fragments are located in positions 1, 3, 5 and 7 of the construct, the presence of two, three and four  $^6\text{FNIII}$  unfolding peaks ensures that at least one, two and three EH-segment inserts must lie within the segment pulled, respectively. Due to the sample preparation (adsorption of the molecule on the substrate on non-defined sites), if two (three and four)  $^6\text{FNIII}$ -unfolding peaks are observed, there can be that one, two or three (two, three or four and three or four) EH-segment inserts must have been pulled. When only one  $^6\text{FNIII}$  unfolding peak is observed, there can be none, one or two EH segments that are stretched (see insets in Figure 5(c)). By comparison between the fingerprints obtained on the poly-protein  $(^6\text{FNIII-EH})_4$  and those measured on the homomeric poly-protein  $(^6\text{FNIII})_8$ , it is clear that the presence of an EH segment in the  $(^6\text{FNIII-EH})$  traces is manifested by an elongation of the initial length  $L_0$ . Stretch curves revealed, on occasion, abrupt force reductions (as can be seen on curve 4 in Figure 5(c)), but they were not seen consistently (they were absent in  $\sim 99\%$  of the curves) and may not be a typical feature of the EH segment, whatever the pulling speeds used (500 nm/s as well as 250 nm/s, 1000 nm/s and 2000 nm/s (data not shown)). This suggests that no stable structures are formed that can withstand detectable levels of force during

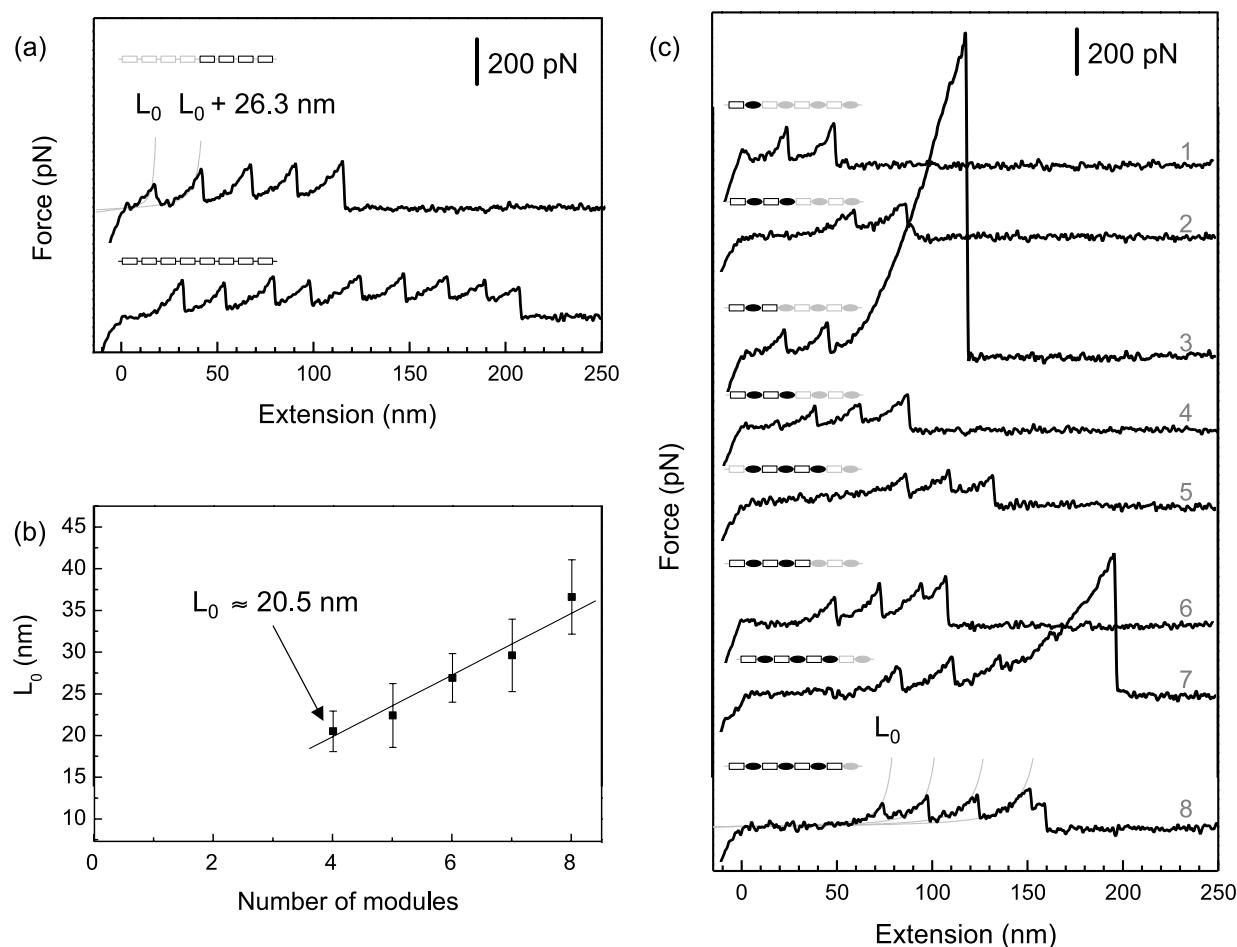


**Figure 5.** Identification and measurement of the elasticity of an EH segment. (a) Characteristic fingerprints of  $^6\text{FNIII}$  domain unfolding by a stretching force, showing different number of sawteeth, depending on the number of modules picked up by the AFM tip recorded at a pulling speed of 500 nm/s. The squares in black represent the modules being picked up in this particular experiment. The continuous lines are fits of the WLC model of polymer elasticity to the data.  $L_0$  is the contour length of the fully folded poly-protein; upon module unfolding at about 160 pN, an additional 26.3 nm will be added to the contour length of the protein. (b) Relationship between  $L_0$ , determined from the fit to the first sawtooth, and the number of modules picked up by the AFM tip, determined by the number of sawteeth while stretching ( $^6\text{FNIII}$ )<sub>8</sub> proteins. The continuous line is a linear regression of the data with a slope of 3.7 nm/module. (c) Stretching of a ( $^6\text{FNIII-EH}$ )<sub>4</sub> poly-protein produces a sawtooth pattern only after an initial spacer  $L_0$ . The sawtooth peaks are typical for  $^6\text{FNIII}$  domain unfolding because they occur at  $\sim 160$  pN and extend the protein by  $\sim 26.3$  nm (pulling speed of 500 nm/s). The discrete values of  $L_0$  result from stretching one, two or three EH segments before any  $^6\text{FNIII}$  module unfolding occurs. The diagrams of the poly-protein accompanying each record show the various combinations of modules picked up by the AFM tip, where squares and circles in black represent  $^6\text{FNIII}$  and EH segments being picked up, respectively. The initial part of the force-extension curve is fitted with the WLC model (equation (1)) to obtain the spring parameters of the EH domain. For the curve 8, a persistence length  $p$  of 0.50 nm, and a contour length  $L_0$  of 86 nm, is obtained. In this example, the tether contains three EH domains and four  $^6\text{FNIII}$  modules.

stretching (forces must be below our AFM noise level (30 pN)). Earlier experimental studies, as well as theoretical studies based on steered molecular dynamics simulations (SMD), indicate that the force required to unfold a domain is highly dependent on the topology of the H-bonds within the protein fold (so dependent on the protein structure).<sup>34–36,44,52,53</sup> It was shown that the interactions that resist mechanical unfolding in an  $\alpha$ -helix (calmodulin) are much weaker than those maintaining the structure of a zipper† H-bonded  $\beta$ -sandwich (C2A

domain), which is in turn less stable than a shear‡ H-bonded  $\beta$ -sandwich topology (titin I27§, corresponding to I91|| in AJ277892). Particularly, calmodulin displayed pure entropic spring behavior without detectable force peaks with AFM.<sup>34</sup> Although the secondary structure composition of the EH segment has not yet been experimentally determined, the analysis of the human EH segment (see Materials and Methods) predicts that at least

† Each H-bond breaks sequentially.

‡ Strand parallel to the direction of the applied force.  
§ Nomenclature of Labeit S. & Kolmerer B. (1995).<sup>11</sup>  
|| Nomenclature of Bang M.-L. *et al.* (2001).<sup>10</sup>

two-thirds of the residues may be unstructured, a few residues ( $<10\%$  of the total) participate in  $\beta$ -strand formation and the rest of the residues form  $\alpha$ -helical structures. The structure predicted for the EH segment, limited  $\alpha$ -helix and largely disordered, is consistent with the absence of force transitions imputable to EH segments when stretching the poly-protein  $({}^6\text{FNIII-EH})_4$  by AFM.

The mechanical properties of the EH fragment are represented by the featureless part of the force-extension relationships, before any of the  ${}^6\text{FNIII}$  domains unfold, that could be fitted with the WLC model of elasticity (gray lines superimposed on the stretch curve 8 in Figure 5(c)). The initial contour length  $L_0$  ranges from 20 nm to 130 nm, which corresponds to the stretching of one (traces 1 and 3), two (traces 2, 4 and 6) or three EH segments (traces 5, 7 and 8), as it can be seen in Figure 5(c). No trace with the stretching of four EH segments has been recorded (due to the fact that the probability of measuring it is very low). The histogram of the initial length  $L_0$  (Figure 6(a)) exhibits three different distinct peaks centered at about  $39(\pm 10)$  nm,  $71(\pm 9)$  nm and  $105(\pm 5)$  nm. Thus, this distribution can be explained by assuming that the initial length  $L_0$  occurs at approximately integer multiples of about  $36(\pm 10)$  nm, distance close to the expected length of an unfolded 96 amino acid residues EH segment ( $96 \times 0.38$  nm). The histogram of persistence lengths (Figure 6(b)) shows a distribution, which is centered at  $\sim 0.3$  nm ( $\sim 0.29(\pm 0.11)$  nm,  $n=182$ ). Persistence length values are in the range of 0.1–0.95. In our case, the distribution seems not to be multimodal as for the cardiac titin PEVK and N2B.<sup>22,25,28</sup> It is interesting to note that the single molecule persistence length of the EH segment is similar to that of unfolded  ${}^6\text{FNIII}$  and  ${}^{10}\text{Ig}$  domains.

EH segment displays non-linear elasticity, is much more compliant than the  ${}^6\text{FNIII}$  and  ${}^{10}\text{Ig}$

domains and its extension occurs at low force and without any significant barriers limiting its extensibility. These results suggest that the EH segment behaves as a random polypeptide chain under force. However, we cannot exclude the possibility that the EH segment may contain structured elements that were not detectable by our AFM. So, the PEVK domain of the I-band of titin was thought to be a pure random coil,<sup>22,24,25</sup> but, in a recent study, using a two-bead optical tweezers assay, Leake *et al.*<sup>28</sup> showed that the persistence length of the PEVK region is dependant on the ionic strength and on temperature, suggesting that this region may not be a pure random coil and contains structured elements.

### Myomesin molecules

Here, we show that myomesin molecules are composed of modules (Ig and FNIII) that are designed to withstand force. Both, the flexible filamentous shape and the mechanical properties of the structural elements of myomesin shown here indicate that, like titin, myomesin is adapted to bear mechanical stress. This view is consistent with the fact that M-line proteins must be stretched and coiled up during muscle contraction and extension since the bridges that myomesin proteins form between thick filaments are oriented nearly perpendicular to the long axis of the thick filament.<sup>7</sup> So, during muscle extension, sarcomere length increases, leading to the extension of the I-band of titin whereas simultaneously inter-filament spacings decrease, releasing tension on the M-band proteins. During muscle contraction, sarcomere length decreases, leading to the coiling of the I-band of titin whereas simultaneously inter-filament spacings increase, stretching the M-band proteins.

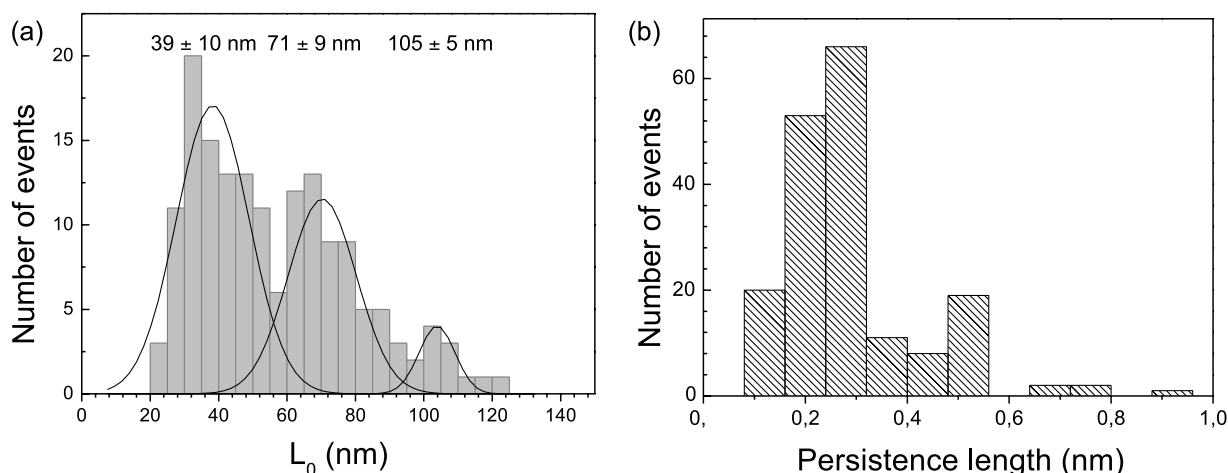


**Figure 6.** (a) Frequency histogram of the initial contour-length distribution of a single  $({}^6\text{FNIII-EH})_4$  poly-protein examined by AFM. The distribution shows three separated peaks ( $n=160$  recordings). Gaussian fits give distributions that peak at 39, 71 nm and 105 nm. The average  $L_0$  of one EH domain is 36 nm. (b) Histogram of the persistence length distribution of the EH segment extracted from measurements on single  $({}^6\text{FNIII-EH})_4$  poly-proteins. The persistence length is distributed around 0.3 nm.

We demonstrate that the EH segment functions like an additional elastic stretch in the middle part of the EH-myomesin protein and behaves like a random coil. Our results indicate that the structural components of the human EH-myomesin have different ability to resist force and have different persistence lengths. The bending rigidity of the native Ig and FNIII segments are likely to be much higher than that of the EH segment (by assuming a persistence length value of about 15 nm for the Ig and FNIII domains in their folded state (according to Higuchi *et al.*<sup>54</sup>) and of 0.3 nm for the EH segment), Ig and FNIII domains elongate at lower forces (without being unfolded), whereas at higher forces and greater stretch, the EH segment unravels as a random coil.

In conclusion, both myomesin isoforms (molecules with or without the EH segment) have different elastic properties, EH-myomesin being the more elastic one. Thus the compliance of the M-band increases with the amount of EH-myomesin it contains. According to the molecular composition of the sarcomeric M-band, which correlates with muscle fiber type,<sup>31</sup> the more compliant M-bands are present in embryonic heart, whereas the less elastic ones are present in fast muscle type. We provide here the evidence that not only titin but also other sarcomeric proteins have complicated visco-elastic properties depending on the contractile parameters in different muscle types.

## Materials and Methods

### Expression of the different constructs

The general method of the preparation of the poly-proteins is the following: the monomers (<sup>6</sup>FNIII, <sup>10</sup>Ig and <sup>6</sup>FNIII-EH), carrying the Aval restriction site (CTCGGG) on both ends, are produced by polymerase chain reaction (PCR) from the human myomesin cDNA. After digestion, the sticky-ended monomers are gel-purified and then self-ligated at high concentration (in order to avoid circular concatemers). These multimers are ligated into self-constructed pET Aval vector. Ligation products are then separated by analytical electrophoresis in an agarose gel and stained with ethidium bromide. The recombinase-deficient *Escherichia coli* strains are used for both cloning and expression of poly-proteins. Clones bearing high-order multimers are selected and transformed into a recombinase-defective strain to express the poly-protein. Purification is done by affinity chromatography using Ni<sup>2+</sup>-column, which binds the His-tagged protein. The purity and monodispersity of proteins are checked by SDS-PAGE and size-exclusion chromatography (HPLC).<sup>34,50</sup> The proteins are stored in phosphate-buffered saline (PBS) buffer, containing 5 mM DTT.

The final construct contained eight, nine and four direct repeats of the <sup>6</sup>FNIII domain, <sup>10</sup>Ig domains and (<sup>6</sup>FNIII-EH) domains, respectively, an amino-terminal His tag for purification, and two carboxyl-terminal Cys codons.

### Mechanical manipulation of poly-proteins

Dynamic force spectroscopy measurements were performed using a commercial atomic force microscope (AFM) instrument (Nanoscope III, Digital Instruments, Santa Barbara, CA). Acquisition of the cantilever deflection data and control of the piezoelectric positioner were done by means of a PCI-MIO-16XE-10 data-acquisition board driven by LabVIEW software (National Instruments, Austin, TX) in connection with an additional personal computer and a home-built high voltage amplifier. The program allowed us to repeatedly unfold and refold one molecule. The cantilevers used in this study are silicon nitride (Si<sub>3</sub>Ni<sub>4</sub>) cantilevers from Olympus (with typical spring constants of ~30 and ~6 pN/nm) and from Park Scientific (with typical spring constants of ~10 pN/nm). Calibration of the spring constants of all cantilevers is done in the experimental buffer and using the equipartition theorem<sup>55</sup> with an absolute uncertainty of 20%.

(<sup>6</sup>FNIII)<sub>8</sub> and (<sup>10</sup>Ig)<sub>9</sub> proteins are allowed to adsorb to freshly evaporated gold surfaces or to pre-cleaned glass microscope slides from a 50 μl drop of a 10–30 μg/ml solution in PBS (pH 7.2, 150 mM NaCl). After the incubation process (~two hours for gold surfaces and 20 minutes for pre-cleaned glass microscope slides) the sample is rinsed with PBS. Similar results are obtained on both substrates.

(<sup>6</sup>FNIII-EH)<sub>4</sub> proteins (50 μl drop of a 1 μg/ml solution in PBS) are allowed to bind to a pre-cleaned glass microscope slide for one minute in PBS. Unbound molecules are washed away with PBS buffer. We optimize the likelihood of stretching single molecules using protein concentrations that were so low that, during continuous probing of the surface with the AFM, only few contacts are made (5 to 10% when stretching (<sup>6</sup>FNIII)<sub>8</sub> and (<sup>10</sup>Ig)<sub>9</sub>, less than 0.5% when studying (<sup>6</sup>FNIII-EH)<sub>4</sub>).

All measurements are performed in PBS buffer (pH 7.2) using an additional of 5 mM dithiothreitol (DTT Fluka). Although the microscope stage was not thermostatted, the room temperature was regulated and always in the range 23–25 °C.

### Treatment and analysis of experimental data

We employed a series of steps in our analysis of single-molecule force data. We corrected the raw force-extension curves for several factors: (1) determination of the zero-length, zero-force data point from the force response that corresponded to the cantilever tip reaching (or departing from) the substrate surface; (2) correction for baseline slope using the force response of the displaced but unloaded cantilever; (3) calculation of the end-to-end length ( $x$ ) of the tethered molecule by correcting the cantilever base displacement ( $s$ ) with cantilever bending (ratio of force ( $F$ ) and cantilever stiffness ( $k$ )) as:

$$x = s - \frac{F}{k}$$

and (4) using the worm-like chain (WLC) equation<sup>43</sup> to model the force *versus* extension characteristics of the unfolded polypeptide, in which  $p$  is the persistence length that describes the polymer stiffness,  $L$  is the contour length, or total length of the polymer backbone,  $k_B$  is Boltzmann's constant,  $T$  is the temperature in Kelvin, and  $x$  is the distance between the ends of the polymer:

$$F(x) = \frac{k_B T}{p} \left( \frac{1}{4(1-x/L)^2} - \frac{1}{4} + \frac{x}{L} \right) \quad (1)$$

## Structure predictions

We used the following programs: PELE and GOR4<sup>†</sup> and nnPredict.<sup>‡</sup>

## Acknowledgements

P.B. gratefully acknowledges the financial support by the National Swiss Foundation and by the Roche Research Foundation.

## References

- Clark, K. A., McElhinny, A. S., Beckerle, M. C. & Gregorio, C. C. (2002). Striated muscle architecture: an intricate web of form and function. *Annu. Rev. Cell Dev. Biol.* **18**, 637–706.
- Horowitz, R. & Podolsky, R. J. (1987). The positional stability of thick filaments in activated skeletal muscle depends on sarcomere length: evidence for the role of titin filaments. *J. Cell Biol.* **105**, 2217–2223.
- Tskhovrebova, L. & Trinick, J. (2003). Titin: properties and family relationships. *Nature Mol. Cell Biol.* **4**, 679–689.
- Gregorio, C. C., Granzier, H., Sorimachi, H. & Labeit, S. (1999). Muscle assembly: a titanic achievement? *Curr. Opin. Cell Biol.* **11**, 18–25.
- Granzier, H. & Labeit, S. (2002). Cardiac titin: an adjustable multi-functional spring. *J. Physiol.* **541–542**, 335–342.
- Freiburg, A., Trombitas, K., Hell, W., Cazorla, O., Fougerousse, F., Centner, T. *et al.* (2000). Series of exon-skipping events in the elastic spring region of titin as the structural basis for myofibrillar elastic diversity. *Circ. Res.* **86**, 1114–1121.
- Obermann, W. M. J., Gautel, M., Weber, K. & Fürst, D. O. (1997). Molecular structure of the sarcomeric M band: mapping of titin and myosin binding domains in myomesin and the identification of a potential regulatory phosphorylation site in myomesin. *EMBO J.* **16**, 211–220.
- Van der Ven, P. F. M., Obermann, W. M. J., Weber, K. & Fürst, D. O. (1996). Myomesin, M-protein and the structure of the sarcomeric M-band. *Advan. Biophys.* **33**, 91–99.
- Trinick, J. & Tskhovrebova, L. (1999). Titin: a molecular control freak. *Trends Cell Biol.* **9**, 377–380.
- Bang, M.-L., Centner, T., Fornoff, F., Geach, A. J., Gotthardt, M., McNabb, M. *et al.* (2001). The complete gene sequence of titin, expression of an unusual ( $\approx 700$ -kDa titin isoform, and its interaction with obsurin identify a novel Z-line to I-band linking system. *Circ. Res.* **89**, 1065.
- Labeit, S. & Kolmerer, B. (1995). Titins: giant proteins in charge of muscle ultrastructure and elasticity. *Science*, **270**, 293–296.
- Trombitas, K., Redkar, A., Centner, T., Wu, Y., Labeit, S. & Granzier, H. (2000). Extensibility of isoforms of cardiac titin: variation in contour length of molecular subsegments provides a basis for cellular passive stiffness diversity. *Biophys. J.* **79**, 3226–3234.
- Linke, W. A., Ivemeyer, M., Olivieri, N., Kolmerer, B., Rüegg, J. C. & Labeit, S. (1996). Towards a molecular understanding of the elasticity of titin. *J. Mol. Biol.* **261**, 62–71.
- Linke, W. A., Rudy, D. E., Centner, T., Gautel, M., Witt, C., Labeit, S. & Gregorio, C. C. (1999). I-band titin in cardiac muscle is a three-element molecular spring and is critical for maintaining thin filament structure. *J. Cell Biol.* **146**, 631–644.
- Trombitas, K., Greaser, M., Labeit, S., Jin, J.-P., Kellermeyer, M., Helmes, M. & Granzier, H. (1998). Titin extensibility *in situ*: entropic elasticity of permanently folded and permanently unfolded molecular segments. *J. Cell Biol.* **140**, 853–859.
- Helmes, M., Trombitas, K., Centner, T., Kellermeyer, M., Labeit, S., Linke, W. A. & Granzier, H. (1999). Mechanically driven contour-length adjustment in rat cardiac titin's unique N2B sequence: titin is an adjustable spring. *Circ. Res.* **84**, 1339–1352.
- Scott, K. A., Steward, A., Fowler, S. B. & Clarke, J. (2002). Titin; a multidomain protein that behaves as the sum of its part. *J. Mol. Biol.* **315**, 819–829.
- Kellermayer, M. S. Z., Smith, S. B., Granzier, H. L. & Bustamante, C. (1997). Folding-unfolding transitions in single titin molecules characterized with laser tweezers. *Science*, **276**, 1112–1115.
- Tskhovrebova, L., Trinick, J., Sleep, J. A. & Simmons, R. M. (1997). Elasticity and unfolding of single molecules of the giant muscle protein titin. *Nature*, **387**, 308–312.
- Rief, M., Gautel, M., Oesterhelt, F., Fernandez, J. M. & Gaub, H. E. (1997). Reversible unfolding of individual titin immunoglobulin domains by AFM. *Science*, **276**, 1109–1112.
- Carrion-Vazquez, M., Oberhauser, A. F., Fowler, S. B., Marszalek, P. E., Broedel, S. E., Clarke, J. & Fernandez, J. M. (1999). Mechanical and chemical unfolding of a single protein: a comparison. *Proc. Natl Acad. Sci. USA*, **96**, 3694–3699.
- Li, H., Oberhauser, A. F., Redick, S. D., Carrion-Vazquez, M., Erickson, H. P. & Fernandez, J. M. (2001). Multiple conformations of PEVK proteins detected by single-molecule techniques. *Proc. Natl Acad. Sci. USA*, **98**, 10682–10686.
- Linke, W. A., Kulke, M., Li, H., Fujita-Becker, S., Neagoe, C., Manstein, D. J. *et al.* (2002). PEVK domain of titin: an entropic spring with actin-binding properties. *J. Struct. Biol.* **137**, 194–205.
- Li, H., Linke, W. A., Oberhauser, A. F., Carrion-Vazquez, M., Kerkvliet, J. G., Lu, H. *et al.* (2002). Reverse engineering of the giant muscle protein titin. *Nature*, **418**, 998–1002.
- Watanabe, K., Nair, P., Labeit, D., Kellermayer, M. S. Z., Greaser, M., Labeit, S. & Granzier, H. (2002). Molecular mechanics of cardiac titin's PEVK and N2B spring elements. *J. Biol. Chem.* **277**, 11549–11558.
- Watanabe, K., Muhle-Goll, C., Kellermayer, M. S. Z., Labeit, S. & Granzier, H. (2002). Different molecular mechanics displayed by titin's constitutively and differentially expressed tandem Ig segments. *J. Struct. Biol.* **137**, 248–258.
- Fisher, T. E., Oberhauser, A. F., Carrion-Vazquez, M., Marszalek, P. E. & Fernandez, J. M. (1999). The study of protein mechanics with the atomic force microscope. *Trends Biochem. Sci.* **24**, 379–384.
- Leake, M. C., Wilson, D., Gautel, M. & Simmons, R. M.

<sup>†</sup> Both available at [workbench.sdsc.edu](http://workbench.sdsc.edu)

<sup>‡</sup> Available at [www.expsy.org](http://www.expsy.org)

- (2004). The elasticity of single titin molecules using a two-bead optical tweezers assay. *Biophys. J.* **87**, 1112–1135.
29. Steiner, F., Weber, K. & Fürst, D. O. (1999). M band proteins myomesin and skelemin are encoded by the same gene: analysis of its organization and expression. *Genomics*, **56**, 78–89.
30. Price, M. G. (1987). Skelemins: cytoskeletal proteins located at the periphery of M-discs in mammalian striated muscle. *J. Cell Biol.* **104**, 1325–1336.
31. Agarkova, I., Auerbach, D., Ehler, E. & Perriard, J.-C. (2000). A novel marker for vertebrate embryonic heart, the EH-myomesin isoform. *J. Biol. Chem.* **275**, 10256–10264.
32. Best, R. B., Brockwell, D. J., Toca-Herrera, J. L., Blake, A. W., Smith, D. A., Radford, S. E. & Clarke, J. (2003). Force mode atomic force microscopy as a tool for protein folding studies. *Anal. Chim. Acta*, **479**, 87–105.
33. Takano, H., Kenseth, J. R., Wong, S.-S., O'Brien, J. C. & Porter, M. D. (1999). Chemical and biochemical analysis using scanning force microscopy. *Chem. Rev.* **99**, 2845–2890.
34. Carrion-Vazquez, M., Oberhauser, A. F., Fisher, T. E., Marszalek, P. E., Li, H. & Fernandez, J. M. (2000). Mechanical design of proteins studied by single-molecule force spectroscopy and protein engineering. *Prog. Biophys. Mol. Biol.* **74**, 63–91.
35. Carrion-Vazquez, M., Marszalek, P. E., Oberhauser, A. F. & Fernandez, J. M. (1999). Atomic force microscopy captures length phenotypes in single proteins. *Proc. Natl Acad. Sci. USA*, **96**, 11288–11292.
36. Yang, G., Cecconi, C., Baase, W. A., Vetter, I. R., Breyer, W. A., Haack, W. A. *et al.* (2000). Solid-state synthesis and mechanical unfolding of polymers of T4 lysozyme. *Proc. Natl Acad. Sci. USA*, **97**, 139–144.
37. Rief, M., Gautel, M., Schemmel, A. & Gaub, H. E. (1998). The mechanical stability of immunoglobulin and fibronectin III domains in the muscle protein titin measured by atomic force microscopy. *Biophys. J.* **75**, 3008–3014.
38. Oberhauser, A. F., Marszalek, P. E., Erickson, H. P. & Fernandez, J. M. (1998). The molecular elasticity of the extracellular matrix protein tenascin. *Nature*, **393**, 181–185.
39. Oberdörfer, Y., Fuchs, H. & Janshoff, A. (2000). Conformational analysis of native fibronectin by means of force spectroscopy. *Langmuir*, **16**, 9955–9958.
40. Oberhauser, A. F., Badilla-Fernandez, C., Carrion-Vazquez, M. & Fernandez, J. M. (2002). The mechanical hierarchies of fibronectin observed with single-molecule AFM. *J. Mol. Biol.* **319**, 433–447.
41. Leake, M. C., Wilson, D., Bullard, B. & Simmons, R. M. (2003). The elasticity of single kettin molecules using a two-bead laser-tweezers assay. *FEBS Letters*, **535**, 55–60.
42. Rief, M., Fernandez, J. M. & Gaub, H. E. (1998). Elastically coupled two-level systems as a model for biopolymer extensibility. *Phys. Rev. Letters*, **81**, 4764–4767.
43. Bustamante, C., Marko, J. F., Siggia, E. D. & Smith, S. (1994). Entropic elasticity of  $\lambda$ -phage DNA. *Science*, **265**, 1599–1600.
44. Rief, M., Pascual, J., Saraste, M. & Gaub, H. E. (1999). Single molecule force spectroscopy of spectrin repeats: low unfolding forces in helix bundles. *J. Mol. Biol.* **286**, 553–561.
45. Evans, E. & Ritchie, K. (1999). Strength of a weak bond connecting flexible polymer chains. *Biophys. J.* **76**, 2439–2447.
46. Zhang, B. & Evans, J. S. (2001). Modeling AFM-induced PEVK extension and the reversible unfolding of Ig/FNIII domains in single and multiple titin molecules. *Biophys. J.* **80**, 597–605.
47. Zhang, B., Xu, G. & Evans, J. S. (1999). A kinetic molecular model of the reversible unfolding and refolding of titin under force extension. *Biophys. J.* **77**, 1306–1315.
48. Fernandez, J. M. & Li, H. (2004). Force-clamp spectroscopy monitors the folding trajectory of a single protein. *Science*, **303**, 1674–1678.
49. Oberhauser, A. F., Hansma, P. K., Carrion-Vazquez, M. & Fernandez, J. M. (2001). Stepwise unfolding of titin under force-clamp atomic force microscopy. *Proc. Natl Acad. Sci. USA*, **98**, 468–472.
50. Li, H., Oberhauser, A. F., Fowler, S. B., Clarke, J. & Fernandez, J. M. (2000). Atomic force microscopy reveals the mechanical design of a modular protein. *Proc. Natl Acad. Sci. USA*, **97**, 6527–6531.
51. Best, R. B., Li, B., Steward, A., Daggett, V. & Clarke, J. (2001). Can non-mechanical proteins withstand force? Stretching barnase by atomic force microscopy and molecular dynamics simulation. *Biophys. J.* **81**, 2344–2356.
52. Lu, H., Isralewitz, B., Krammer, A., Vogel, V. & Schulten, K. (1998). Unfolding of titin immunoglobulin domains by steered molecular dynamics simulation. *Biophys. J.* **75**, 662–671.
53. Marszalek, P. E., Lu, H., Li, H., Carrion-Vazquez, M., Oberhauser, A. F., Schulten, K. & Fernandez, J. M. (1999). Mechanical unfolding intermediates in titin modules. *Nature*, **402**, 100–103.
54. Higuchi, H., Nakauchi, Y., Maruyama, K. & Fujime, S. (1993). Characterization of B-connectin (Titin 2) from striated muscle by dynamic light scattering. *Biophys. J.* **65**, 1906–1915.
55. Hutter, J. L. & Bechhoefer, J. (1993). Calibration of atomic-force microscopic tips. *Rev. Sci. Instrum.* **64**, 1868–1873.

Edited by M. Moody

(Received 22 October 2004; received in revised form 13 March 2005; accepted 14 March 2005)